

Performance of Solar Domestic Hot Water Systems at the National Bureau of Standards— Measurements and Predictions

A. H. Fanney

Solar Equipment Group,
National Bureau of Standards,
Washington, D.C. 20234

S. A. Klein

Guest Worker,
National Bureau of Standards,
Solar Energy Laboratory,
University of Wisconsin,
Madison, Wis. 53706

The thermal performance of six solar domestic hot water systems and a conventional hot water system have been carefully monitored by the National Bureau of Standards in Gaithersburg, Maryland. The system configurations include an evacuated-tube air system with a crossflow heat exchanger and two storage tanks, a single-tank direct system, a double-tank direct system, a single-tank indirect system with a wrap-around heat exchanger, a double-tank indirect system with a coil-in-tank heat exchanger, and a thermosyphon system. Results are presented for a one-year time interval commencing January 1980. This paper includes a detailed description of the hot-water systems, experimental test results, and comparisons with computer predictions using the f-chart method [1].

Introduction

The National Bureau of Standards (NBS) solar domestic hot water (SDHW) test program has two primary objectives. One objective is to investigate alternative methods of testing SDHW systems [2] to support the American Society of Heating, Refrigerating and Air Conditioning Engineers (ASHRAE) in developing a standard test procedure [3]. A second objective is to conduct controlled experiments on typical solar domestic water heaters to determine the extent to which existing computer programs and design methods accurately predict their performance.

The controlled experiments began in June 1978 with the gathering of detailed performance data on six heavily instrumented SDHW systems at the NBS solar test site in Gaithersburg, Maryland. All systems were run side-by-side under identical meteorological conditions and each provided approximately 0.265 m³ of hot water per day. Operational results for the first 12 months are reported in [4]. Comparisons were made between the results and the predictions of TRNSYS [5], f-CHART [6], and SOLCOST [7]. A description of these comparisons for the first 12 months appears in reference [8].

After completion of the first 12-months test of the six systems at the end of June, 1979, modifications were made to the systems in preparation for the next 12 months of tests. An evacuated-tube air collector system was installed in place of the flat-plate air collector system. A preheat storage tank with an internal-coil heat exchanger replaced the tank with the wrap-around heat exchanger in the double-tank indirect system. An additional collector panel was added to the single-tank direct (drain-down) system to make its collector area

identical with other liquid systems, and the tanks for the double-tank direct system were replaced by tanks with additional insulation. Also, mixing valves at the hot water outlet were removed from all six systems. The necessary

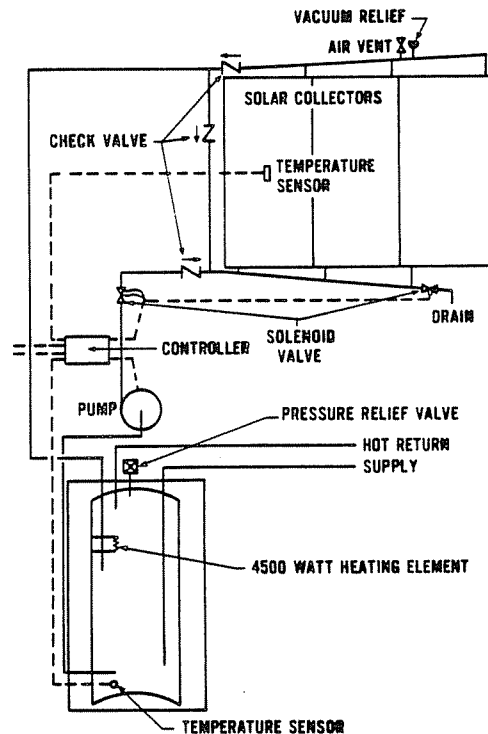


Fig. 1 NBS single-tank direct system

Contributed by the Solar Energy Division and presented at the ASME Solar Energy Conference, Orlando, Florida, April 18-27, 1983. Manuscript received by the Solar Energy Division October 22, 1982.

modifications, instrumentation, and calibration were completed by December 1979.

This paper summarizes the results of the second 12-month testing period between January 1980 and December 1980. Presented are a description of each of the systems and the instrumentation used to monitor their performance. Measurements of the collector performance characteristics, storage tank heat loss coefficients, heat exchanger effectiveness values for the two indirect systems, and storage tank temperature profiles are included. Comparisons are made between the experimental results and predictions using the f -Chart method.

System Description

The SDHW test facility consists of six independent solar systems. A complete description of each system follows.

Single-Tank Direct System. The configuration of the single-tank direct system is shown in Fig. 1. This system consists of three solar collectors connected in parallel, one water storage tank, flow control valves, an on-off differential temperature controller with freeze protection circuitry, pump, piping, and insulation.

The collectors used on all five liquid systems are Lennox Model LSC18-1S.¹ This is a single-glass cover flat-plate liquid collector. The glass is tempered low iron with etched surface lines to reduce reflection. A steel absorber plate is formed around copper flow tubes and then coated with black chrome.

¹Certain commercial equipment, instruments, or materials are identified in this paper in order to adequately specify the experimental procedure. Such identification does not imply recommendation or endorsement by the National Bureau of Standards nor does it imply that the materials or equipment identified are necessarily the best available for the purpose. The results of this study apply to the particular systems tested. Generalization of these results to generic types of SDHW systems is not necessarily possible.

Each collector has an aperture area of 1.40 m². The collector enclosure is constructed of galvanized steel lined with 89 mm of glass fiber insulation. Instantaneous efficiency tests of the Lennox LSC18-1S collectors were performed at NBS. A least-squares curve fit to the data, based on aperture area, resulted in a linear efficiency of

$$\eta_A = 0.805 - 4.73 ((t_{fi} - t_u) / G_T) \quad (1)$$

The measured incident angle modifier is represented by

$$K_{\tau\alpha} = 1.0 - 0.10 [(\cos \theta)^{-1} - 1] \quad (2)$$

A State Industries conventional electric water heater is used for storage. This tank has a nominal 310L capacity and outside dimensions of 1.57 m in height by 0.61 m in diameter. The inner surface of the tank is lined with vitrified glass to minimize corrosion. Glass fiber insulation, thickness 51 mm, surrounds the actual storage tank, which in turn is covered by a thin metal jacket. A temperature and pressure relief valve is located at the top of the storage tank. The lower heating element was not used in this experiment. The upper heating element, located 1.27 m above the tank bottom is a 208 volt, 3.5 kW, direct immersion heating element. The heating element is controlled by a thermostat which senses the temperature of the storage tank immediately above it. The solar-heated water enters the tank through a 12.7-mm dia dip tube extending 153 mm below the upper heating element.

The overall heat loss coefficient for each storage tank was determined experimentally. During a 72-hr cool-down test, no energy was supplied or withdrawn from the storage tanks. Each tank was initially heated to 70°C. The ambient temperature surrounding the storage tanks was maintained at 20°C. Using readings from thermocouples located inside and surrounding the storage tanks, a plot of average tank temperature versus time was generated. Fitting an exponential curve to the resulting data allowed the overall heat loss

Nomenclature

e = fractional energy savings excluding parasitic energy, dimensionless	Q_{SHE} = energy consumed by the heating elements in the solar system, kJ
e_{AUX} = fractional energy savings including parasitic energy, dimensionless	Q_{TL} = thermal tank losses of a conventional electric hot water tank, kJ
e_H = fractional energy savings calculated using the f -Chart correlation and measured horizontal radiation data, dimensionless	Q_{TLS} = energy loss for the auxiliary portion of the solar system, kJ
e_T = fractional energy savings calculated using the f -Chart correlation and measured tilt radiation data, dimensionless	t_a = ambient temperature, °C
f = solar fraction, dimensionless	$t_{c,in}$ = collector fluid temperature entering the heat exchanger, °C
F_R' / F_R = collector-heat exchanger correction factor, dimensionless	$t_{c,out}$ = collector fluid temperature leaving the heat exchanger, °C
$F_R (\tau\alpha)_n$ = intercept of collector efficiency curve based on aperture area, dimensionless	t_{fi} = fluid temperature entering the solar collector array, °C
$F_R U_L$ = slope of the collector efficiency curve based on aperture area, (W/(m ² - °C))	t_l = average water temperature in the solar-heated portion of the storage tank, °C
G_T = total global irradiance incident upon the aperture plane of the collector array, W/m ²	UA_{TLS} = energy loss coefficient for the auxiliary portion of the solar system, W/°C
\bar{H} = monthly average daily total radiation incident upon a horizontal surface, MJ/m ² -day	ϵ_c = heat exchanger effectiveness, dimensionless
\bar{H}_d = monthly average daily diffuse radiation incident upon a horizontal surface, MJ/m ² -day	θ = angle of incident between the direct solar beam and the normal to the collector aperture, deg
\bar{H}_t = monthly average daily total radiation on the solar collector array, MJ/m ² -day	η_A = collector efficiency based on aperture area, dimensionless
$K_{\tau\alpha}$ = incident angle modifier, dimensionless	η_g = collector efficiency based on gross area, dimensionless
Q_{AUX} = energy consumed by pump, controls, and solenoid valves if applicable, kJ	$(\tau\alpha)_n$ = effective transmittance-absorptance product for the collector at normal incidence, dimensionless
Q_{CONV} = energy required by a conventional hot water system, kJ	$(\bar{\tau\alpha})$ = monthly average transmittance-absorptance product for the collector, dimensionless
Q_{LS} = hot water thermal load of the solar system, kJ	

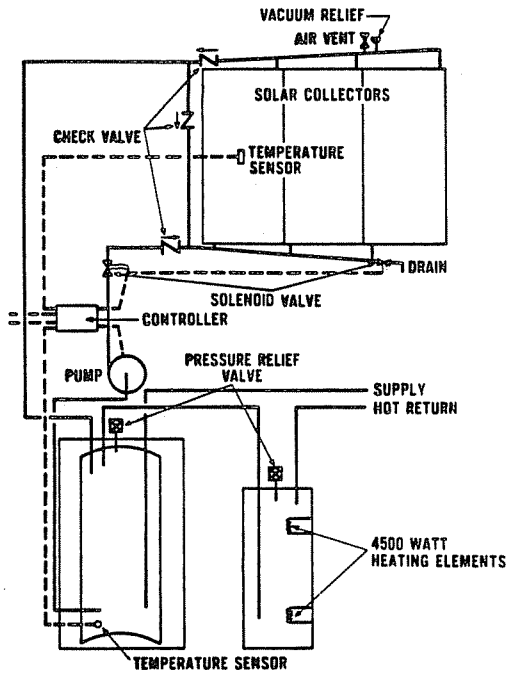


Fig. 2 NBS double-tank direct system

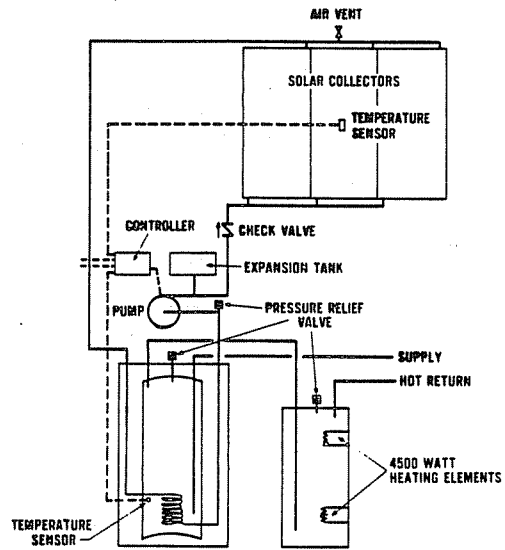


Fig. 4 NBS double-tank indirect system

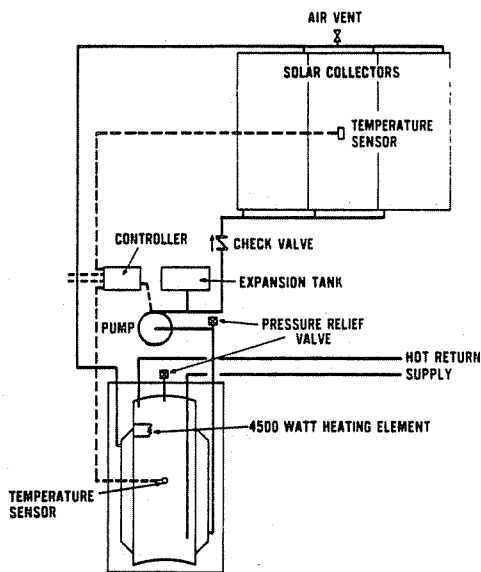


Fig. 3 NBS single-tank indirect system

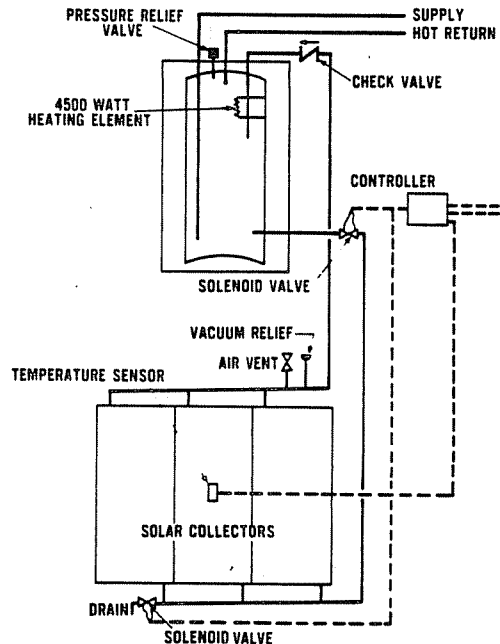


Fig. 5 NBS thermosyphon system

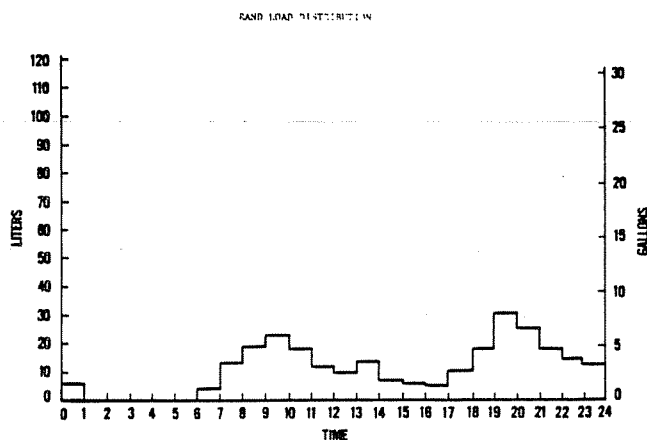
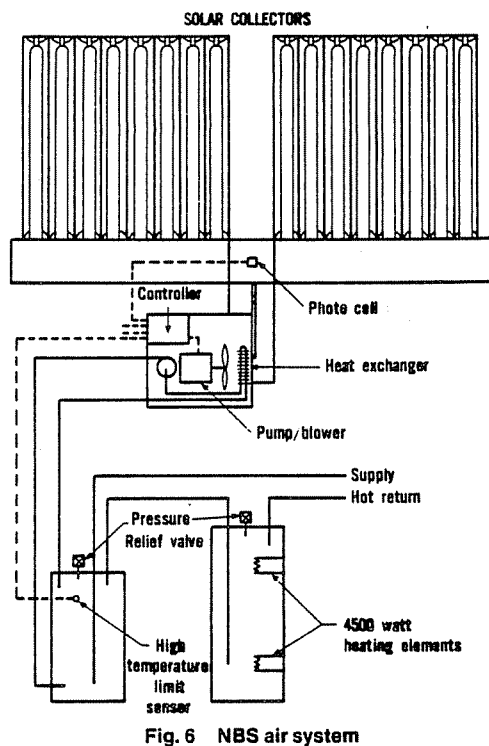
coefficient to be determined for each tank. For the single-tank direct system, the measured overall heat loss coefficient is 4.42 W/°C. A Hawthorne Model 1504-A Fix Flow controller is used to actuate the Grundfos UPS-20-42 pump when a temperature difference of 8.9°C exists between the collector absorber plate and the storage tank temperatures. A temperature difference of less than 1.7°C causes circulation to cease. The collector flow rate is at 0.0833 L/s. The storage tank sensor is located on the exterior tank surface, at an elevation of 0.152 m. The controller also actuates two solenoid valves to provide freeze protection. Freeze protection action is initiated if the absorber plate temperature reaches 2.8°C. One solenoid valve closes the supply to the collectors while the second one opens and allows drainage of the collectors. A fail-safe scheme is employed such that during a power failure the collector supply is closed and the collector drain is opened. An air vent and a vacuum relief valve attached to the highest point of the system allow venting of air

during collector fill and eliminates a partial vacuum in the collectors during a drainage.

Hard copper tubing of 12.7-mm dia is used throughout the installation, except for 25.4-mm dia headers interconnecting the three collectors. Armaflex insulation of 12.7 mm provide indoor type insulation. Outdoor insulation consists of 32-mm thick glass fiber insulation covering the 12.7-mm piping while a 51-mm glass fiber insulation encases the collector headers.

Double-Tank Direct System. The double-tank direct system is shown in Fig. 2. This system consists of three solar collectors connected in parallel, two water storage tanks, flow control valves, an on-off differential temperature controller with freeze protection circuitry, a pump, and associated piping.

Lennox LSC18-1S solar collectors are utilized. Both the preheat and auxiliary storage tank are A. O. Smith Energy Saver III conventional electric hot water tanks. The two heating elements in the 303-L heating elements are utilized to maintain the 151-L auxiliary tank at 60°C. Outside dimensions of the 303-L tank are 1.50 m in height by 0.56 m in diameter. The 151-L tank has outside dimensions of 1.4 m in



height by 0.56 m in diameter. Both storage tanks are surrounded by glass fiber insulation having a thickness of 64 mm. The measured overall heat loss coefficients for the preheat tank and auxiliary tank are, respectively, 3.31 W/°C and 2.03 W/°C.

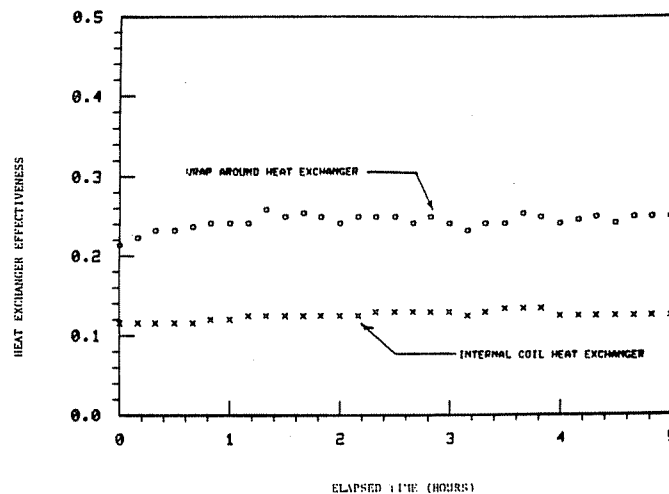
A Hawthorne Model 1504-A Fix Flo controller regulates the Grundfos UPS-20-42 pump and freeze protection unit. All components and control temperature set-points are identical to those utilized in the single-tank direct system. The collector flow rate is 0.0833 L/s. Piping and insulation are identical to the single tank direct system.

Single-Tank Indirect System. The single-tank, closed-loop indirect system, Fig. 3, consists of three Lennox Model LSC18-1S collectors connected in parallel, a single water storage tank, an on-off differential temperature controller, a pump, and associated piping and insulation.

The Solarstream 310-L water storage tank has an integral 4500-W heating element located in the upper portion of the tank. Thus, during periods of insufficient solar energy, the

Table 1 Monthly source water temperature and average ambient temperature

Month	Ambient [°C]	Mains [°C]
Jan.	0.0	8.2
Feb.	0.0	9.6
Mar.	6.1	10.4
Apr.	12.4	12.5
May.	19.3	17.7
Jun.	20.1	19.1
Jul.	25.0	19.5
Aug.	24.0	24.9
Sept.	21.2	26.1
Oct.	11.1	20.8
Nov.	6.0	13.1
Dec.	0.3	10.4



heating element set at 60°C satisfies the load requirements. The outside dimensions of this tank are 1.42 m in height by 0.71 m in diameter. A double-wall heat exchanger jacket surrounding the water tank allows the heat transfer fluid to heat the water within. The heat transfer fluid is a mixture of ethylene glycol (40 percent by weight) and distilled water with a specific heat of 3.60 kJ/kg°C and specific gravity of 1.042 at 40°C. The heat exchanger jacket has an area of 1.58 m² that is attached to the surface of the tank by mechanical bonding. Insulation surrounding the heat exchanger and tank consists of 76-mm thick glass fiber. A 76-mm insulation slug also exists at the top and bottom of the tank. The measured overall heat loss coefficient for this tank is 3.02 W/°C.

A Honeywell Model R7412A Controller for this tank actuates the Grundfos UPS-20-42 pump when a temperature difference of 10°C exists between the absorber plate and a tank surface temperature sensor. The tank sensor is located at a height of 0.7 m. A 1.7°C temperature difference causes the 0.0833 L/s circulation to terminate.

Piping and insulation are identical to that of the systems previously discussed systems.

Double-Tank Indirect System. The double-tank indirect closed-loop system, Fig. 4, uses three Lennox Model LSC18-1S collectors connected in parallel, two water storage tanks, an on-off differential temperature controller, and a Grundfos UPS-20-40, two-speed pump. A Ford Model TC80E stone-lined storage tank with an internal coil double-wall heat exchanger serves as the preheat tank. Outside dimensions of the tank are 1.68 m in height and 0.61 m in diameter. Glass fiber insulation, 51 mm in thickness, surrounds the storage tank. The measured overall heat loss coefficient is 2.95 W/°C for this tank. The downstream auxiliary tank is identical to the auxiliary tank of the double-tank direct system. The

pump circulates an ethylene glycol-water (40 percent-60 percent) mixture at 0.0833 L/s. A Honeywell differential temperature controller, identical to the single tank indirect system controller, is employed. The tank temperature sensor is located at a height of 0.432 m on the preheat storage tank under the glass fiber insulation. Piping and insulation are identical to the previously discussed systems.

Thermosyphon System. The thermosyphon system consists of three Lennox Model LSC18-1A collectors connected in parallel, one water storage tank, and a freeze protection system (Fig. 5).

The water storage tank is a 250-L State Industries conventional electric hot water tank. The bottom 4500-W heating element has been disconnected for this experiment, while the upper 4500-W electric heating element maintains the upper portion of the stored water at 60°C. The measured overall heat loss coefficient for the tank is 4.62 W/°C.

Freeze protection is provided by utilizing solenoid valves and a controller to operate in the same fashion as those utilized in the single and double-tank direct systems. A Hawthorne 1504-A Controller provides the needed freeze protection circuitry. Two solenoid valves, one which closes the collector inlet and one which drains the collector, are actuated at a 2°C absorber plate temperature. A check valve on the collector return piping prevents reverse thermosyphoning as well as tank drainage during freeze periods.

Hard copper tubing of 25.4-mm dia is used exclusively on the collector flow loop. All piping bends were kept to a minimum in order to minimize pressure drops throughout the system. Armaflex insulation of 13-mm thickness provides interior plumbing insulation. Exterior insulation consists of a 51-mm glass fiber insulation encasing all piping.

Air System. The General Electric TCA Solar Hot Water System is shown in Fig. 6. Two collector modules are connected by center feed to an energy transfer module (ETM). Each solar collector module consists of eight evacuated tube assemblies backed by curved reflectors. Air enters each assembly between the inner surface of the evacuated tube and the outer surface of a return tube. At the end of each evacuated tube, the air is diverted into the interior of the return tube gaining additional heat. At the end of the return tube the air is delivered to the hot air duct. The ETM contains a motor attached to both a blower and a water pump and also contains an air-to-water heat exchanger. The gross area of the two collectors including the center feed duct work is 3.92 m².

The two TCA collectors and ETM were tested as a unit by DSET Laboratories [9]. A least squares fit to the test data resulted in the following efficiency equation of

$$\eta_g = 0.370 - 0.511 \left[\frac{t_{fi} - t_a}{G_T} \right] - 0.17 \left[\frac{t_{fi} - t_a}{G_T} \right]^2 \quad (3)$$

based on gross area. The measured combined incident angle modifier is represented by

$$K_{\tau\alpha} = 1.0 - 0.21 \left(\frac{1}{\cos\theta} - 1 \right) \quad (4)$$

The water flowing through the ETM circulates through a State Industries 114-L storage tank. Outside dimensions of this tank are 1.0 m in height by 0.46 m in diameter. The measured overall heat loss coefficient for this tank is 2.64 W/°C. The auxiliary tank is a 159-L State Industries conventional electric hot water tank. Both 4500-W heating elements are utilized to maintain the set-point temperature. Outside dimensions of the 159-L tank are 1.22 m in height by 0.51 m in diameter. Glass fiber insulation, thickness 51 mm, surrounds the actual storage tank resulting in a measured overall heat loss coefficient of 2.80 W/°C.

The controller activates the ETM if the solar intensity,

measured by a photodiode, is greater than 158 W/m². If the preheat tank temperature exceeds the high-temperature cut-off limit, 80°C, the controller deactivates the unit.

Inlet Water Temperature Control System. The inlet water temperatures to all six SDHW values are listed in Table 1. The temperature of the water is controlled by means of 310-L storage tank with one 4500-W integral heating element in combination with a 0.75-ton chiller. When a hot water draw takes place, water from a well located at the test site replenishes the 310-L tank. The water is circulated continuously around a closed loop post the inlet of each system, and through the chiller and the 310-L tank. A temperature controller interfaced with the electric heating element supplies the energy required to heat the water if necessary. A thermostat incorporated in the chiller actuates the chiller to remove heat, if so required. The inlet water temperature control system maintains the set-point temperature to within a tolerance of ±2°C.

Automated Hot Water Draw System. The outlet of each hot water system interconnects with a main header. A normally closed solenoid valve, located at the center of the header, releases the flow to a drain when actuated. An electronic timer combined with a stepping relay selects an interval timer corresponding to the desired hourly draw. The automatic reset interval timers range from 1.5 to 10 min in duration. A constant flow valve control located at the exit of each system is set to maintain a flow rate of 3.79 L/min when the solenoid valve is open. Thus, when a given interval timer is energized for its set-time interval, a corresponding amount of water is drawn from each of the six systems. A flow totalizer at the exit of the interconnecting header totalizer the draw down from all six systems. The Rand load schedule [10], Fig. 7, was used in this experimental program.

Instrumentation. Each SDHW system is extensively instrumented. Located within each water storage tank are Type T copper-constantan thermocouples spaced in 152-mm increments along a vertical axis. Thermocouples also monitor the collector inlet and outlet temperature for each system. The inlet and exit potable water temperatures are measured with thermocouples, and a three-junction thermopile measures the temperature difference between the inlet and outlet during draw down.

A General Electric type I-70-S kWh meter is used to measure the auxiliary energy consumed by the electric heating elements. A Duncan Electric Model EM 10 Wh meter measures the energy used by the circulators, controls, solenoid valves, etc., for each system. The water consumption of each system is measured by two Badger Meter Model 15 flow totalizers. A Brooks Instrument Company Rotometer measures the flow rate of the fluid circulating through the collectors of each liquid system. A three-valve bypass arrangement is included on each liquid system such that a turbine flowmeter may be installed in the collector flow loop. This capability allows the flow rate to be continuously recorded if desired for any system. An elapsed time meter connected to each system's controller measures the amount of time the circulators are in operation.

Recorded meteorological information includes horizontal surface radiation, tilted surface radiation, wind speed, wind direction, and ambient temperature. The SDHW test facility has a total of 150 independent inputs which are measured every 10 min by a Leeds & Northrup Trendscan 1000 High Sensitivity Data Acquisition Unit. The data acquisition system is interfaced with a Kennedy Model 1600/360 incremental-write magnetic tape recorder. The magnetic tape is replaced every seven days and taken to the NBS computer center for data reduction.

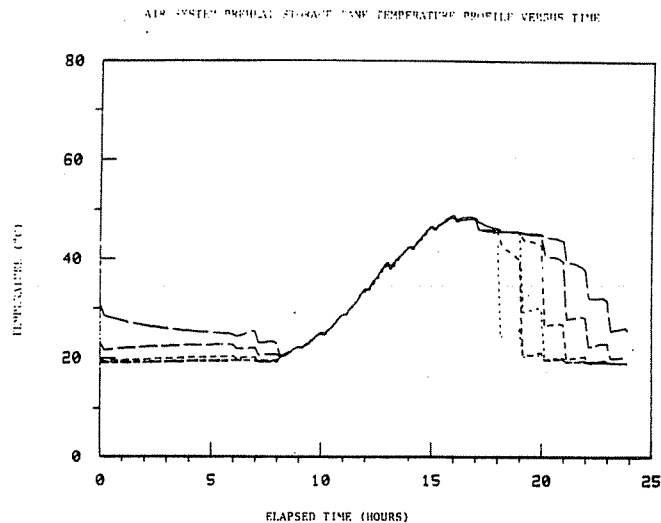


Fig. 9 Air system preheat storage tank temperature profile versus time

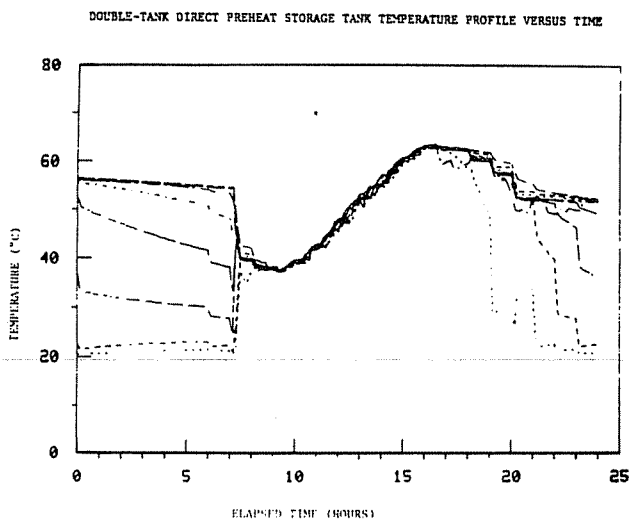


Fig. 10 Double-tank direct preheat storage tank temperature profile versus time

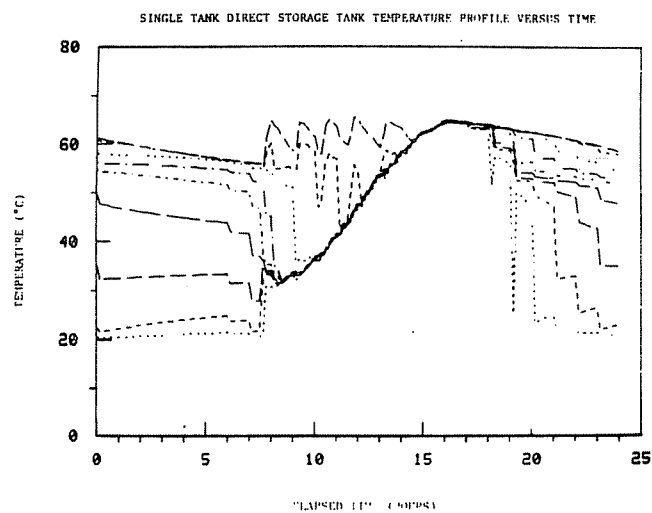


Fig. 11 Single-tank direct storage tank temperature profile versus time

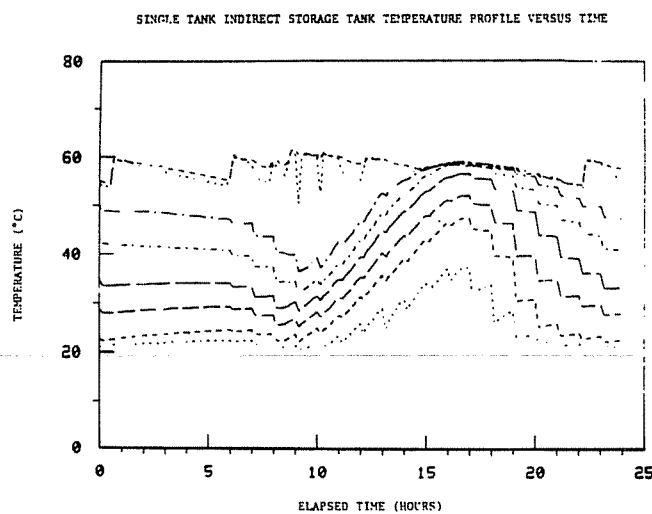


Fig. 12 Single-tank indirect storage tank profile versus time

Experimental Results

Heat Exchanger Effectiveness. The air, single-tank, and double-tank indirect systems utilized a heat exchanger to provide heat transfer between the collector fluid and the potable water within the storage tanks. The efficiency curve for the air system, equation (3), includes the effect of the air-to-water heat exchange. For the single- and double-tank indirect systems the heat exchanger effectiveness is needed in order to compare experimental system performance to predictions using the f -Chart method.

The heat exchanger effectiveness was determined in the following manner. The two storage tanks were initially filled with 23°C water. The collector heat transfer fluid rates were maintained at 0.0833 L/s throughout a five hour test interval. The inlet and outlet temperatures of each heat exchanger and the temperature of the water within the storage tanks were measured at 10-min intervals. For each 10-min interval, the effectiveness of the heat exchanger was calculated using the following relationship

$$\epsilon_c = \frac{t_{c,in} - t_{c,out}}{t_{c,in} - t_t} \quad (5)$$

where $t_{c,in}$ and $t_{c,out}$ are the temperatures of the collector fluid entering and exiting the heat exchanger, respectively, and t_t is the average water temperature in the solar-heated portion of

the storage tank. For the double-tank indirect system the average preheat tank temperature represents, t_t . For the single-tank indirect system, the solar heated portion of the tank is defined as the portion of the storage tank surrounded by the wrap-around heat exchanger.

Figure 8 shows the effectiveness the single-tank indirect wrap-around heat exchanger and the double-tank indirect coil-in-tank heat exchanger as a function of time. The average tank temperature varied from 23°C initially for both tanks to a final temperature of 55°C for the single-tank indirect and 48°C for the double-tank indirect system. Heat exchanger effectiveness values of 0.24 and 0.13 were selected, based on these experimental data, as representing typical values of the single-tank indirect and double-tank indirect systems.

Stratification. Vertical tank temperature profiles within each storage tank were measured using copper-constantan thermocouples positioned every 152 mm along the vertical axis of each tank. Figures 9–14 show the temperature profiles in the solar storage tanks for May 30, 1980.

The preheat tank for the air and double-tank direct systems exhibit similar temperature profiles as seen in Figs. 9 and 10. The degree of stratification which exists within these storage tanks is dependent upon the operational status of the circulator pumps. During time intervals when the pumps are not energized, the tanks are stratified. During periods of solar energy collection, the circulation of water through the storage

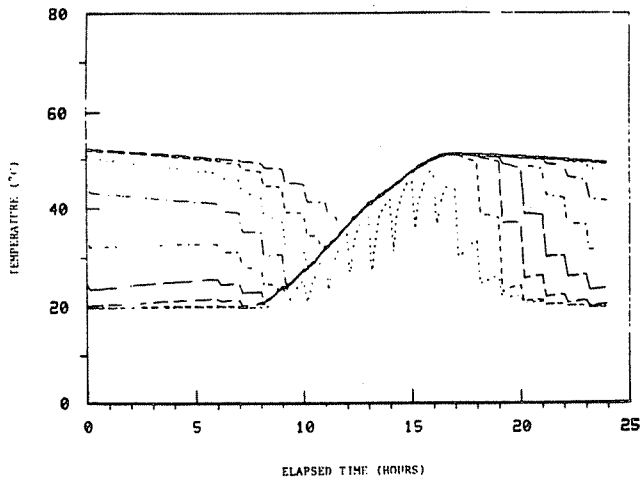


Fig. 13 Double-tank indirect preheat storage tank temperature profile versus time

tanks resulted in rapid mixing of the water in each tank. After thirty minutes of continuous circulator operation, no stratification exists within the storage tanks.

The temperature profile for the single-tank direct system is shown in Fig. 11. Good stratification is maintained during periods of no solar energy collection. When circulation through the storage tank commences, the portion of the tank monitored by the lower seven thermocouples rapidly becomes well mixed. The upper thermocouple, located above the heating element, shows a rapid decay in temperature followed by a rapid increase in temperature during operation of the circulating pump. This rapid temperature decay is due to mixing between the lower solar heated portion of the tank and the upper auxiliary heated portion of the tank. As the temperature in the upper portion of the tank continues to decrease the thermostat energizes the electric heating element, resulting in a rapid temperature increase. The rate of temperature decay for the auxiliary heated portion is significantly less during periods of no solar energy collection due to the lack of mixing within the storage tank.

The single-tank indirect system temperature profile, Fig. 12, displays excellent stratification over the entire day. The preheat tank of the double-tank indirect system, however, displays a temperature profile, Fig. 13, similar to the preheat tank temperature profiles for the air and double-tank direct systems. The large difference in stratification characteristics between the two indirect systems is probably due to the manner in which heat is transferred to the water within the storage tanks. The wrap-around heat exchanger distributes heat around the outer surface of the tank. The internal-coil heat exchanger is a more localized heat source, and it produces a heat flux which appears to induce convective currents within the tank resulting in a well-mixed tank.

Stratification within the thermosyphon storage tank is excellent, as seen in Fig. 14. The lack of mixing within the thermosyphon system during periods of solar energy collection is due to the small flow rate through the solar collector array.

The temperature of the water in the auxiliary tanks of the double-tank systems, not shown, is uniform. This well-mixed condition exists because both heating elements within each tank maintain the temperature at 60°C.

SDHW System Performance. A comparison between the performance of each solar hot water system and that of a conventional hot water system meeting the same thermal load

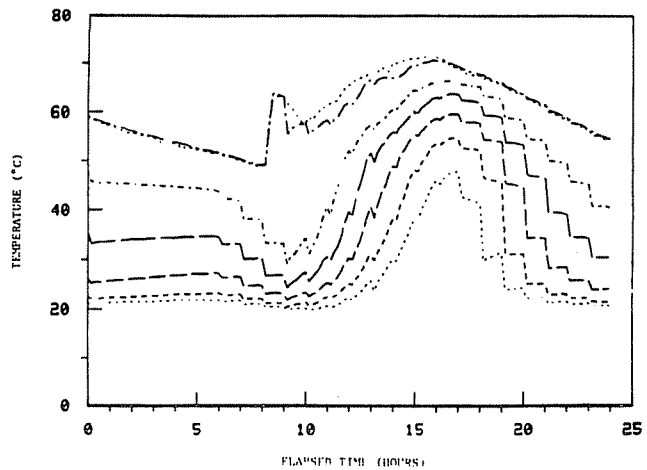


Fig. 14 Thermosyphon storage tank temperature profile versus time

requirement is possible by defining a parameter called the "fractional energy savings," i.e.,

$$e_{AUX} = 1 - \frac{Q_{SHE} + Q_{AUX}}{Q_{CONV}} \quad (6)$$

where e_{AUX} is the fractional energy savings of the solar system including parasitic power required to operate the system, Q_{SHE} is the energy consumed by the heating elements in the solar systems, Q_{AUX} is the energy consumed by pump, controls, and solenoids if applicable, and Q_{CONV} is the quantity of energy supplied by a conventional hot water system meeting the same load requirements. The energy consumed by a conventional hot water system is computed using

$$Q_{CONV} = Q_{LS} + Q_{TL} \quad (7)$$

where Q_{LS} is the actual hot water thermal load of the solar system, and Q_{TL} is the thermal tank losses of a conventional electric hot water tank. Comparisons in this paper are based on a conventional tank having losses of 11,160 kJ per day.

A second fractional energy savings, e , can be computed if the parasitic energy consumption of the solar system is ignored.

$$e = 1 - \frac{Q_{SHE}}{Q_{CONV}} \quad (8)$$

This parameter is useful in making comparisons to the f -Chart predictions, since no parasitic power is accounted for using the f -Chart method.

Table 2 gives the fractional energy savings, including and excluding parasitic energy, for each solar system for the twelve month test period. An error analysis conducted in accordance with Kline and McClintock [11] results in a probable error, for the range of fractional energy savings encountered, of ± 1.5 percentage points. The thermosyphon system provided the greatest fractional energy savings. The evacuated tubular air system provided only 24 percent, including parasitic power, of the energy required by a conventional water heater. Consistent with earlier studies at NBS [8], the single-tank systems out-performed the double-tank systems. All components of the two direct systems, with the exception of storage tanks, are identical. Over the 12-month test period, the single-tank direct system provided 53 percent of the energy required for a conventional water heater compared to 50 percent for the double-tank direct system. The double-tank direct system, however, has a greater capability to meet thermal loads during periods of insufficient solar irradiance. A thermal performance comparison of single

Table 2 Fractional energy savings of six SDHW systems, percent^a

Month	Single-tank direct	Double-tank direct	Single-tank indirect	Double-tank indirect	Double-tank air	Single-tank thermosyphon
Jan.	34.5 (31.5)	34.4 (31.1)	33.9 (32.1)	29.3 (27.2)	21.6 (18.4)	45.7 (43.3)
Feb.	51.9 (48.1)	53.0 (49.0)	53.9 (51.2)	42.8 (40.2)	30.8 (26.3)	67.0 (64.5)
Mar.	53.0 (48.2)	47.1 (42.1)	48.6 (46.0)	42.9 (39.9)	26.9 (22.3)	56.6 (53.2)
Apr.	61.3 (55.3)	62.0 (55.5)	67.1 (63.7)	53.4 (49.9)	37.0 (30.6)	76.1 (72.0)
May.	65.5 (58.9)	61.1 (53.7)	66.5 (62.6)	53.3 (51.3)	32.9 (26.2)	71.9 (67.1)
June	73.5 (66.0)	66.4 (58.1)	70.9 (66.6)	55.9 (51.3)	36.2 (28.1)	78.2 (73.2)
July	80.8 (73.5)	74.0 (65.8)	73.1 (68.7)	60.2 (55.6)	38.9 (30.4)	82.4 (77.6)
Aug.	74.5 (66.7)	70.5 (60.9)	65.6 (60.8)	53.7 (48.4)	33.9 (25.2)	72.0 (66.5)
Sept.	78.5 (70.5)	74.5 (64.5)	73.0 (68.6)	51.0 (46.0)	35.6 (26.6)	77.7 (72.3)
Oct.	65.4 (59.0)	61.4 (54.4)	53.9 (50.7)	37.8 (34.2)	30.1 (23.7)	60.7 (56.4)
Nov.	50.9 (47.2)	51.1 (46.4)	47.9 (45.7)	34.0 (31.5)	27.7 (23.7)	48.5 (45.8)
Dec.	35.9 (32.7)	40.9 (36.6)	39.6 (37.7)	39.6 (36.9)	20.3 (16.6)	55.0 (52.9)
Entire Year	58.4 (53.0)	55.7 (49.6)	55.5 (52.4)	44.8 (41.4)	29.9 (24.2)	65.1 (61.2)

^aNumbers in parentheses include parasitic energy use

Table 3 Input data for the *f*-chart calculations

	STD	DTD	STI	DTI	AIR
A [m ²]	4.19	4.19	4.19	4.19	3.92
$F_R(\tau\alpha)_n$	0.805	0.805	0.805	0.805	0.37 ^a
$F_R U_L$ [W/m ² ·°C]	4.73	4.73	4.73	4.73	0.51 ^a
$K_{\tau\alpha}$	Eq. (2)	Eq. (2)	Eq. (2)	Eq. (2)	Eq. (4)
ϵ_s	1.0	1.0	0.24	0.13	1.0
F_R'/F_R	1.0	1.0	0.833	0.702	1.0
$(UA)_{TLS}$ [W/°C]	1.10	2.02	0.98	1.97	2.80
T_{set} [°C]	60	60	60	60	60

^aIncludes F_R'/F_R factor
(Monthly mains and ambient temperatures appear in Table 1.)

versus double-tank indirect systems can not be made based on this study since different heat exchangers are utilized. A previous study at NBS [8], where identical heat exchangers were used, resulted in the single-tank indirect system out performing the double-tank indirect system.

Parasitic energy use resulted in a reduction in fractional energy savings from 3 to 6 percent. The effect of parasitic energy use on the fractional energy savings is greater for the direct systems as compared to the indirect systems because of fail-safe freeze protection scheme used by the direct systems requiring two solenoid valves to be energized continuously during nonfreeze conditions.

Operational Problems. Hardware problems related to the operation of the SDHW test facility during the 12-month test period included failure of the controller on the air system and failure of the solenoid valves on the drain-down systems.

Failure of solenoid valves on the single-tank direct, double-tank direct, and thermosyphon systems resulted in three categories of problems. Failure of the solenoid isolation valve to close during freezing conditions, thereby not isolating the storage tank(s) from the collector array, resulted in large amounts of water being lost through the collector drain. Failure of solenoid drain valves to open on the collector array during freeze conditions resulted in burst manifold pipes and a burst riser tube on one collector panel. Additionally, cracks in the diaphragm located inside the solenoid valve on the collector arrays resulted in leaks developing at the collector array drain during nonfreeze conditions.

Comparison of Experimental and Calculated Performance

The *f*-chart method [1] is widely used to estimate the long-term performance of solar water heating systems. Although it was originally developed for double-tank systems having an external heat exchanger, comparisons with computer simulations have shown that the *f*-Chart method can be applied for single-tank systems and for systems in which the heat exchange coil is located within the storage tank [12]. The *f*-Chart method should, therefore, be applicable to all of the

solar water heating systems investigated except the thermosyphon system. The *f*-Chart calculations presented below were made in the manner outlined in [1] with the following modifications.

(i) As recommended in [12], the load used in the *f*-Chart calculations was the sum of Q_{LS} , the energy required to heat the water from the main supply to the set temperature, and Q_{TLS} , the auxiliary tank energy loss. For double-tank systems, Q_{TLS} was calculated as the product of the auxiliary tank energy loss coefficient, $(UA)_{TLS}$, and the difference between the set and tank environment temperatures integrated over the period of operation. The auxiliary energy loss for single-tank systems was assumed to occur from the portion of the tank above the heating element; Q_{TLS} was calculated in the same manner as for double-tank systems, except that $(UA)_{TLS}$ was estimated to be the product of the energy loss coefficient for the single-tank and the fraction of the tank area from which auxiliary losses occur. The solar fraction, f , obtained from the *f*-Chart correlation is the fraction of total load ($Q_{LS} + Q_{TLS}$) supplied by solar energy. The auxiliary energy, Q_{SHE} , needed in addition to the solar contribution to supply the load is then $(1-f)(Q_{LS} + Q_{TLS})$. Final calculation results are expressed in terms of the fractional energy savings, e , defined in equation (8).

(ii) The monthly-average transmittance-absorption product ratio, $(\tau\alpha)/(\tau\alpha)_n$ was estimated as described in [13]. Experimental values of $K_{\tau\alpha}$, the incidence angle modifier, were used to determine the angular dependence of the transmittance-absorption product ratio. The monthly-average diffuse radiation fraction, \bar{H}_d/\bar{H} , needed to estimate $(\tau\alpha)/(\tau\alpha)_n$, was obtained from the correlation developed by Erbs [14].

(iii) The collector-heat exchanger efficiency factor, F_R'/F_R , was assumed to be 1.0 for the two direct systems. F_R'/F_R was also taken to be 1.0 for the air system since the collector test results in equation (3) include the effect of the air-to-water exchanger. For the indirect systems, F_R'/F_R was calculated as described in [1] for external heat exchangers assuming the minimum fluid capacitance rate (mass flow rate, specific heat product) to be the collector fluid capacitance rate.

The collector parameters, $F_R(\tau\alpha)_n$ and $F_R U_L$, were taken to be the *Y*-intercept and negative slope, respectively, of the collector test data represented by equations (1) and (3). Since the *f*-Chart method assumes $F_R U_L$ to be constant, the quadratic term in equation (3) cannot be considered. $F_R U_L$ for the air system is quite small; the effect of neglecting the quadratic term was judged to have little effect on the calculated results.

The input information used to apply the *f*-Chart method is

Table 4 Comparison of experimental and calculated performance for the single-tank direct system

Month	N	\bar{H} [MJ/m ² -day]	\bar{H}_T [MJ/m ² -day]	\overline{HR} [MJ/m ² -day]	Q_{LS} [MJ]	Q_{TLS} [MJ]	e	e_T	e_H
Jan.	27.0	5.77	8.19	8.34	1501.	102.6	0.35	0.30	0.31
Feb.	23.0	10.29	14.75	14.27	1082.	87.4	0.52	0.59	0.57
Mar.	23.9	12.65	14.03	14.48	1300.	90.9	0.53	0.53	0.54
Apr.	18.0	18.80	19.09	19.16	1016.	68.4	0.61	0.68	0.68
May	23.0	19.41	16.51	17.86	1180.	87.2	0.65	0.63	0.67
June	24.0	22.40	18.00	19.70	1115.	91.2	0.73	0.71	0.76
July	19.0	22.35	18.41	20.03	875.	72.2	0.81	0.74	0.79
Aug.	16.0	17.59	16.18	17.05	644.	60.8	0.75	0.68	0.71
Sept.	23.0	16.18	18.34	17.97	898.	87.3	0.79	0.75	0.74
Oct.	17.0	11.49	15.73	14.84	696.	64.6	0.65	0.65	0.62
Nov.	27.0	8.37	12.24	13.08	1455.	102.5	0.51	0.46	0.49
Dec.	18.6	6.54	9.96	10.91	1043.	70.7	0.36	0.36	0.39
Year					12805.	985.9	0.58	0.57	0.58

Table 5 Comparison of experimental and calculated performance for the double-tank direct system

Month	N	\bar{H} [MJ/m ² -day]	\bar{H}_T [MJ/m ² -day]	\overline{HR} [MJ/m ² -day]	Q_{LS} [MJ]	Q_{TLS} [MJ]	e	e_T	e_H
Jan.	26.0	5.93	8.45	8.67	1564.	182.0	0.34	0.25	0.26
Feb.	21.0	10.52	14.99	14.69	1044.	147.0	0.53	0.53	0.52
Mar.	26.9	12.33	13.57	14.04	1652.	188.3	0.47	0.43	0.45
Apr.	18.0	18.80	19.09	19.16	983.	126.0	0.62	0.65	0.65
May	23.0	19.41	16.51	17.86	1123.	160.6	0.61	0.60	0.65
June	24.0	22.40	18.00	19.70	1061.	168.0	0.66	0.68	0.74
July	19.0	22.35	18.41	20.03	811.	133.0	0.74	0.73	0.78
Aug.	16.0	17.59	16.18	17.05	570.	112.0	0.70	0.68	0.71
Sept.	20.0	17.12	17.44	19.18	666.	140.0	0.74	0.73	0.79
Oct.	14.0	11.80	16.20	15.35	627.	98.0	0.61	0.58	0.55
Nov.	25.0	8.31	11.97	12.95	1231.	175.0	0.51	0.43	0.46
Dec.	15.0	6.21	9.24	10.13	740.	104.6	0.41	0.31	0.65
Year					12072.	1734.2	0.56	0.52	0.55

Table 6 Comparison of experimental and calculated performance for the single-tank indirect system

Month	N	\bar{H} [MJ/m ² -day]	\bar{H}_T [MJ/m ² -day]	\overline{HR} [MJ/m ² -day]	Q_{LS} [MJ]	Q_{TLS} [MJ]	e	e_T	e_H
Jan.	27.0	5.77	8.19	8.34	1412.	91.3	0.34	0.29	0.30
Feb.	23.0	10.29	14.75	14.27	1053.	77.7	0.54	0.55	0.53
Mar.	27.0	12.33	13.57	14.04	1401.	91.3	0.49	0.48	0.49
Apr.	18.0	18.80	19.09	19.16	937.	60.8	0.67	0.64	0.65
May	24.0	19.78	16.78	18.20	1117.	81.1	0.66	0.61	0.65
June	22.0	22.84	18.00	20.06	967.	74.4	0.71	0.67	0.72
July	19.0	22.35	18.41	20.03	818.	64.2	0.73	0.70	0.75
Aug.	16.0	17.59	16.18	17.05	554.	54.1	0.66	0.68	0.71
Sept.	23.0	16.18	18.34	17.97	853.	77.3	0.73	0.71	0.70
Oct.	22.0	11.17	14.91	14.31	1003.	74.4	0.54	0.53	0.51
Nov.	30.0	7.99	11.75	12.27	1579.	101.4	0.48	0.41	0.42
Dec.	24.9	5.93	9.76	9.48	1271.	84.2	0.40	0.34	0.33
Year					12965.	932.5	0.55	0.52	0.54

Table 7 Comparison of experimental and calculated performance for the double-tank indirect system

Month	N	\bar{H} [MJ/m ² -day]	\bar{H}_T [MJ/m ² -day]	\overline{HR} [MJ/m ² -day]	Q_{LS} [MJ]	Q_{TLS} [MJ]	e	e_T	e_H
Jan.	27.0	5.77	8.19	8.34	1525.	183.8	0.29	0.20	0.21
Feb.	23.0	10.29	14.75	14.27	1053.	156.6	0.43	0.44	0.43
Mar.	27.0	12.33	13.57	14.04	1551.	183.8	0.43	0.35	0.37
Apr.	18.0	18.80	19.09	19.16	1028.	122.5	0.53	0.50	0.50
May	24.0	19.78	16.78	18.20	1223.	163.4	0.55	0.47	0.51
June	24.0	22.40	18.00	19.70	1152.	163.4	0.56	0.52	0.56
July	19.0	22.35	18.41	20.03	884.	129.4	0.60	0.55	0.60
Aug.	16.0	17.59	16.18	17.05	620.	108.9	0.54	0.52	0.55
Sept.	23.0	16.18	18.34	17.97	897.	156.6	0.51	0.58	0.57
Oct.	22.0	11.17	14.91	14.31	1021.	149.8	0.38	0.42	0.40
Nov.	30.0	7.99	11.75	12.27	1710.	204.2	0.34	0.30	0.31
Dec.	24.9	5.93	9.76	9.48	1271.	169.5	0.40	0.26	0.25
Year					13935.	1892.0	0.45	0.40	0.42

Table 8 Comparison of experimental and calculated performance for the air system

Month	N	\bar{H} [MJ/m ² -day]	\bar{H}_T [MJ/m ² -day]	\overline{HR} [MJ/m ² -day]	Q_{LS} [MJ]	Q_{TLS} [MJ]	e	e_T	e_H
Jan.	27.0	5.77	8.19	8.34	1466.	261.2	0.22	0.11	0.12
Feb.	23.0	10.29	14.75	14.27	1097.	222.5	0.31	0.26	0.25
Mar.	26.9	12.33	13.57	14.04	1468.	231.4	0.27	0.21	0.22
Apr.	18.0	18.80	19.09	19.16	971.	174.1	0.37	0.31	0.32
May	15.0	19.24	16.20	17.71	734.	222.1	0.33	0.28	0.30
June	24.0	22.40	18.00	19.70	1086.	232.2	0.36	0.32	0.36
July	19.0	22.35	18.41	20.03	807.	183.7	0.39	0.36	0.39
Aug.	16.0	17.59	16.18	17.05	581.	154.8	0.34	0.33	0.35
Sept.	23.0	16.18	18.34	17.97	822.	222.2	0.36	0.38	0.37
Oct.	22.0	11.17	14.91	14.31	919.	164.4	0.30	0.27	0.26
Nov.	30.0	7.99	11.75	12.27	1557.	260.9	0.28	0.19	0.20
Dec.	24.9	5.93	9.76	9.48	1315.	180.1	0.20	0.14	0.14
Year					12823.	2600.3	0.30	0.25	0.25

summarized in Table 3 for the five active systems. Comparisons between the experimental and calculated performance of these five systems appear in Tables 4-8. Due to operational problems with the systems and the instrumentation, there are gaps in the experimental data; the number of days for which data were recorded, N , is given in the first column of these tables.

Columns 2 and 3 list the average daily radiation (per unit area) on a horizontal surface and on the collector plane, respectively, over the period for which data were recorded. The solar radiation on the collector plane was also estimated from the horizontal data using the algorithm presented in [15]. In these calculations, the diffuse radiation fraction was obtained from the correlation recommended by Erbs [14] and the ground reflectance was assumed to be 0.2 for all months. The estimated radiation, \overline{HR} , in column 4, is generally in good agreement with the measured radiation on the collector plane, although it is consistently higher during the summer months.

The load, Q_{LS} , appearing in column 5, was obtained by integrating the product of the measured hot water draw rate and the difference between the set and main supply water temperatures over the period for which data were available. The load used in the f -Chart correlation was the sum of Q_{LS} and Q_{TLS} , the auxiliary tank energy loss. Q_{TLS} , appearing in column 6, was estimated as described above.

The experimental value of the fractional energy savings, e , is given in column 7. The fractional energy savings calculated using the f -Chart correlation, appears in the last two columns. The value of e_T was obtained using \bar{H}_T , the measured radiation on the collector surface in column 3 as input; the estimated radiation in column 4 was used to obtain e_H .

Presumably, the results obtained using the measured radiation data on the collector plane (rather than on a horizontal surface) provide a better indication of the accuracy of the f -Chart method. The annual fractional energy savings calculated using the measured solar radiation data are slightly lower (0.01 to 0.05) than the experimental values.

The fractional energy savings calculated using the estimated radiation are of interest since long-term measurements of solar radiation data on tilted surfaces are generally not available. In this case, the performance calculated using the radiation data estimated from the horizontal measurements agrees more closely with the experimental results than that obtained using the measured radiation data on the collector plane.

Discussion

The performance of six different types of SDHW systems has been carefully monitored over a one-year period under identical operating conditions. An intercomparison of the performance of these six systems provides the opportunity for an interesting discussion of some of the design trade-offs in SDHW systems.

An indication of the relative merits of single versus double-tank systems can be seen by comparing the annual fractional energy savings of the single-tank direct and double-tank direct system. These two systems are identical in all respects except for the number of storage tanks. The single-tank system slightly outperformed the double-tank system (58 percent versus 56 percent), presumably because the smaller tank surface area in the single-tank system resulted in less tank energy losses than in the double-tank system. As noted previously, however, the single-tank system has the disadvantage of having less hot water ready for immediate use.

The effect of freeze control strategy is reflected in a comparison of the single-tank direct system with the single-tank indirect system. Excluding parasitic energy use, the direct system performed 3 percent (58 percent versus 55 percent) better than the indirect system. The direct system enjoys a thermal advantage because its performance is not penalized by the collector-tank heat exchanger. However, the indirect system with an antifreeze solution circulating through the collectors required less parasitic energy. It is also a more reliable freeze control strategy. Fewer operational problems were experienced with the indirect systems.

Of the six systems tested, the thermosyphon system required the least amount of auxiliary energy. Three explanations can be offered to account for its excellent performance. First, the thermosyphon system tested is a single-tank system which thus has low thermal energy losses. The storage tank volume of the thermal system was the smallest of the six systems. Second, the thermosyphon system is a direct system and, as a result, it avoids the thermal performance penalty associated with heat exchange between the collector fluid and the stored water. Third, and perhaps most importantly, the small flow rate through the thermosyphon collector array (measured to be less than 0.015 L/s) results in a high degree of thermal stratification in the storage tank with little opportunity for mixing of water heated by the electric heating element with that returning to the collectors.

A comparison of the heat exchanger performance in the single and double tank indirect systems demonstrates that different internal heat exchanger designs can result in markedly different heat exchanger performance. The measured effectiveness of the wrap-around heat exchanger used in the single-tank indirect system was significantly higher than the effectiveness of the coil-in-tank heat exchanger used in the double-tank indirect system. In both systems, the measured effectiveness was found to be insensitive to the temperatures of the stored water and the heated collector fluid. In addition, a higher degree of thermal stratification was observed in the single-tank indirect system, presumably because the plumes of heated water rising from the internal coil promote internal mixing.

One purpose of this investigation was to determine the accuracy with which the f -Chart method could predict the performance of SDHW systems. Using the experimentally

measured monthly meteorological data and hot water loads, along with experimental values of the collector parameters, storage tank loss coefficients, heat exchanger effectiveness, and excluding parasitic energy, the annual solar savings fraction estimated by the *f*-Chart method was within 5 percent of the measured value for the five active systems.

Acknowledgments

This research was sponsored by the Office of Solar Heat Technologies, U.S. Department of Energy, Washington, D.C. 20585. Appreciation is also extended to Charles Terlizzi who operates the SDHW test facility and Catherine A. Scarbrough who wrote the necessary software for reduction of the experimental data.

References

- 1 Beckman, W. A., Klein, S. A., and Duffie, J. A., *Solar Heating Design*, Wiley-Interscience, New York, 1977.
- 2 Fannee, A. H., Thomas, W. C., Scarbrough, C. A., and Terlizzi, C. P., "Analytical and Experimental Analysis of Procedures for Testing Solar Domestic Hot Water Systems," NBS Building Science Series 140, Feb. 1982.
- 3 "Method of Testing to Determine Thermal Performance of Packaged Residential Solar Water Heaters," ASHRAE Standard 95-1981.
- 4 Fannee, A. H., and Liu, S. T., "Performance of Six Solar Domestic Hot

Water Systems in the Mid-Atlantic Region," *Conference Proceedings—Solar Heating and Cooling Systems Operational Results*, 1979, p. 25.

5 "TRNSYS, A Transient Simulation Program," Engineering Experiment Station Report 38-10, University of Wisconsin-Madison, Solar Energy Laboratory, June 1979.

6 "F-CHART-3.0 Users Manual," Engineering Experiment Station, University of Wisconsin-Madison, June, 1978.

7 Connolly, M., Giellis, R., Jensen, C., and McMordie, R., "Solar Heating and Cooling Computer Analysis—A Simplified Design Method for Non-Thermal Specialists," Martin Marietta Corporation, *Proceedings of the Joint Conference of the American Section of the International Solar Energy Society and the Solar Energy Society of Canada*, Winnipeg, Canada, August 15-20, 1976.

8 Fannee, A. H., and Liu, S. T., "Comparing Experimental and Computer-Predicted Performance for Solar Hot Water Systems," *ASHRAE Journal*, May 1980.

9 "Solar Collector Test Report," DSET No. 21270S, Sept. 1979.

10 Mutch, J. J., "Residential Water Heating: Fuel Conservation, Economics and Public Policy," Rand Corporation, R-1498-NSF, May 1974.

11 Kline, S. J., and F. A. McClintock, "Describing Uncertainties in Single-Sample Experiments," *Mech. Eng.*, Jan. 1953, p. 3.

12 Buckles, W. E., and Klein, S. A., "Analyses of Solar Domestic Hot Water Heaters," *Solar Energy*, Vol. 25, 1980, pp. 417-424.

13 Klein, S. A., "Calculation of the Monthly-Average Transmittance-Absorption Product," *Solar Energy*, Vol. 23, 1979, pp. 547-555.

14 Erbs, D. G., Klein, S. A., and Duffie, J. A., "Estimation of the Diffuse Radiation Fraction for Hourly, Daily, and Monthly-Average Global Radiation," *Solar Energy* (in press) 1982.

15 Klein, S. A., and Theilacker, J. C., "An Algorithm for Calculating Monthly-Average Radiation on Inclined Surfaces," *ASME Journal of Solar Energy Engineering*, Vol. 103, Feb. 1981,

